
Molecular Crystals and Liquid Crystals
Publication details, including instructions for authors and subscription information:
http://www.tandfonline.com/loi/gmcl16

# Calculation and Measurement of the Effect of Pressure on Charge Carrier Transport in Naphthalene

M. El Hamamsy [a c], A. C. Damask [a] & S. A. Elnahwy [b d]

[a] Queens College of the City, University of New York, Flushing, New York, 11367

[b] Faculty of Engineering of Cairo University, Cairo, Egypt

[c] Bell Laboratories, Murray Hill, NJ, 07974

[d] Physics Department, Faculty of Science, United Arab Emirates University, P.O. Box 15551, AL AIN, U. A. E.

Version of record first published: 20 Apr 2011.

To cite this article: M. El Hamamsy , A. C. Damask & S. A. Elnahwy (1983): Calculation and Measurement of the Effect of Pressure on Charge Carrier Transport in Naphthalene, Molecular Crystals and Liquid Crystals, 95:3-4, 209-235

To link to this article: http://dx.doi.org/10.1080/00268948308072464

*Mol. Cryst. Liq. Cryst.*, 1983, Vol. 95, pp. 209–235
0026-8941/83/9504–0209/$18.50/0

Printed in the United States of America



# Calculation and Measurement of the Effect of Pressure on Charge Carrier Transport in Naphthalene

M. El HAMAMSY,[†] A. C. DAMASK

*Queens College of the City, University of New York, Flushing, New York 11367*

and

S. A. ELNAHWY[‡]

*Faculty of Engineering of Cairo University, Cairo — Egypt*

*(Received March 18, 1983)*

Intermolecular transfer integrals, including exchange and vibrational effects, for an excess electron and an excess hole in a naphthalene crystal are calculated as functions of pressure using the linear compressibilities. These integrals are then used to calculate the pressure dependence of the band structure, the drift mobility components and the Hall mobility.

A novel design of a non-magnetic high pressure cell with optical windows is described. Hall mobility of an excess hole was measured at high pressure by a photo-injection technique. The results of the calculations give a good agreement with available drift mobility data and with the Hall mobility measured in this work. Comparison between the calculated and observed mobilities shows that the constant mean-free-path approximation is superior to the constant-relaxation-time approximation for naphthalene.

## INTRODUCTION

A number of investigators[1–6] used the tight binding approximation to calculate increasingly more reliable carrier band structures in naphthalene. With these results Leblanc[7] and Friedman[8] calculated the expected behavior of

[†]Now at Bell Laboratories, Murray Hill, NJ 07974.

[‡]Present address: Physics Department, Faculty of Science, United Arab Emirates University, P. O. Box 15551, AL AIN, U. A. E.

the ratio of the Hall mobility to the drift mobility ($\mu_H/\mu_D$). The results of the calculations were not, however, definitive enough in confirming that the charge carriers transport mechanism is a band one. A comprehensive study of the band structure and the drift and Hall mobilities at high pressure is certainly an important step towards the understanding of the conduction mechanism in molecular crystals. In the present work, comprehensive calculations were done for the band structures of an excess electron and an excess hole in a naphthalene crystal. The calculations were done at different pressures using the directly measured linear compressibilities determined by neutron diffraction techniques.[9] These calculations were then used to calculate the components of the drift mobility tensor as functions of pressure in the two approximations of constant relaxation time $\tau$ and constant mean free path $\lambda$. The results of the calculations are in a fairly good agreement with the previously reported experimental data[10–12] as far as the atmospheric pressure anisotropy is concerned especially in the constant $\lambda$ approximation. Hall mobility was also calculated as a function of pressure for the different combinations of directions of the electric and magnetic fields. Hall mobility of an excess hole was measured at high pressure and the results are compared with the calculations which give additional support to the band model in the constant $\lambda$ approximation.

## NUMERICAL CALCULATIONS

The procedure followed in this work for the calculation of the band structure of naphthalene is basically similar to that first introduced by Katz, *et al.*,[3] but with several refinements. First, in the calculation of the molecular wavefunctions, the Hoyland and Goodman[13] coefficients were used and two-and three-center integrals were included in the calculation of the intermolecular resonance integrals. This refinement was used by Elnahwy, *et al.*,[14] in their calculation of the band structure of anthracene. The same numerical approximations made by the latter authors and a modified version, to suit naphthalene, of the computer program were used in this work. Furthermore, exchange and vibrational effects were taken into consideration in the calculation of the intermolecular transfer integrals. This was done following the treatments given by Silbey, *et al.*,[4] and Glaeser and Berry[5] and details are given by El Hamamsy.[15]

The linear compressibilities used in the present calculations are as follows:[9]

$$\frac{1}{a_0}\frac{\partial a}{\partial p} = 0.0056 \qquad \text{kbar}^{-1}$$

$$\frac{1}{b_0}\frac{\partial b}{\partial p} = 0.0032 \qquad \text{kbar}^{-1}$$

$$\frac{1}{c_0}\frac{\partial c}{\partial p} = 0.0026 \qquad \text{kbar}^{-1}$$

$$\frac{1}{\beta}\frac{\partial \beta}{\partial p} = 0.0014 \qquad \text{kbar}^{-1}$$

where $\beta$ is the monoclinic angle, and $a$, $b$, and $c$ are the lattice constants.

### Results for the intermolecular-transfer integrals and band-structure calculations

For the sake of comparison the same molecular labeling scheme of previous investigators,[3] shown in Figure 1, was used in this work. The intermolecular-resonance integrals are given in Table I at different pressures. Table II gives the intermolecular exchange integrals and the vibrational overlap integrals are given in Table III. The latter integrals were calculated from the equation given by Choi, *et al.*,[16] as follows,

$$\langle \chi_i^{00}/\chi_j^{\pm n}\rangle = \frac{1}{(n!)^{1/2}}(\delta_{we}\sqrt{2})^n \exp(-\delta_{we}^2/4)$$

where $\chi^{00}$ represents the zeroth vibrational state of the ground state of the neutral molecule, $n$ the vibrational quantum number of the ion, and $\chi^{\pm n}$ its vibrational state. The parameter $\delta_{we}$ is given by:

$$\delta_{we} = 158.9\sqrt{2}\,(k/\nu)^{1/2}z$$

where $k$ is the force constant corresponding to the vibrational states and $\nu$ their frequencies, $z$ is a factor that characterizes the change in molecular

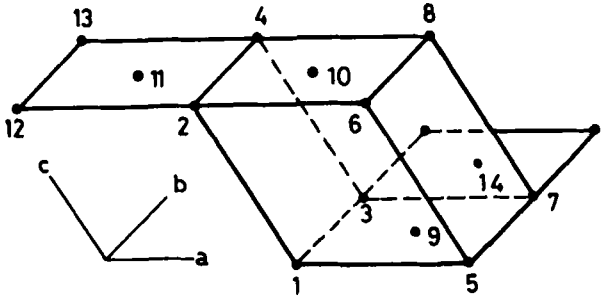


FIGURE 1 Molecular labeling scheme.

TABLE I

Intermolecular resonance integrals (two- and three-center in units of $10^{-4}$ ev.

| Pressure (Kbars) | | | | | | | |
|---|---|---|---|---|---|---|---|
| Molecule # | Atm. | 1.0 | 2.0 | 3.0 | 4.0 | 5.0 | 6.0 |
| | | | Hole | | | | |
| 2 | −0.33 | −0.46 | −0.59 | −0.73 | −0.89 | −1.07 | −1.29 |
| 3 | −127.01 | −132.03 | −137.25 | −142.68 | −148.33 | −154.21 | −160.31 |
| 4 | 0.41 | 0.44 | 0.46 | 0.49 | 0.51 | 0.54 | 0.56 |
| 5 | 0.29 | 0.29 | 0.29 | 0.30 | 0.30 | 0.31 | 0.33 |
| 6 | 10.54 | 11.71 | 12.33 | 13.70 | 15.20 | 16.60 | 18.41 |
| 7 | 0.31 | 0.34 | 0.36 | 0.39 | 0.43 | 0.46 | 0.50 |
| 8 | 0.06 | 0.06 | 0.06 | 0.06 | 0.07 | 0.08 | 0.08 |
| 9 | 31.85 | 34.95 | 38.24 | 41.77 | 45.55 | 49.60 | 53.95 |
| 10 | −39.25 | −42.24 | −45.38 | −48.63 | −51.98 | −55.43 | −59.07 |
| 11 | −0.03 | −0.03 | −0.03 | −0.03 | −0.03 | −0.03 | −0.03 |
| 12 | 0.00 | 0.00 | 0.00 | 0.00 | 0.00 | 0.00 | 0.00 |
| 13 | 0.00 | 0.00 | 0.00 | 0.00 | 0.00 | 0.00 | 0.00 |
| 14 | 0.04 | 0.04 | 0.04 | 0.05 | 0.05 | 0.06 | 0.06 |
| | | | Electron | | | | |
| 2 | −4.97 | −5.63 | −6.34 | −7.10 | −7.91 | −8.78 | −9.69 |
| 3 | 28.33 | 29.72 | 31.16 | 32.67 | 34.25 | 35.91 | 37.67 |
| 4 | 0.07 | 0.07 | 0.07 | 0.07 | 0.08 | 0.08 | 0.09 |
| 5 | −0.05 | −0.05 | −0.04 | −0.06 | −0.08 | −0.10 | −0.12 |
| 6 | 1.62 | 1.87 | 2.01 | 2.33 | 2.68 | 3.21 | 3.68 |
| 7 | −0.07 | −0.08 | −0.08 | −0.09 | −0.09 | −0.09 | −0.10 |
| 8 | −0.03 | −0.04 | −0.04 | −0.04 | −0.04 | −0.04 | −0.04 |
| 9 | −56.91 | −58.77 | −60.63 | −62.51 | −64.41 | −66.34 | −68.28 |
| 10 | −2.43 | −3.16 | −3.93 | −4.71 | −5.49 | −6.35 | −7.22 |
| 11 | −0.03 | −0.03 | −0.03 | −0.03 | −0.04 | −0.04 | −0.04 |
| 12 | 0.00 | 0.00 | 0.00 | 0.00 | 0.00 | 0.00 | 0.00 |
| 13 | 0.00 | 0.00 | 0.00 | 0.00 | 0.00 | 0.00 | 0.00 |
| 14 | 0.01 | 0.02 | 0.02 | 0.02 | 0.02 | 0.02 | 0.02 |

shape. The values of $k$, $\nu$, $z$ used were those given by McCoy and Ross.[17] The intermolecular transfer integrals were calculated from the equation,

$$\text{T.IS} = (\text{I.RS} - \text{IE}) \cdot \text{F}$$

where *T.IS* is the intermolecular transfer integral, *I.RS* is the intermolecular resonance integral, *IE* is the intermolecular exchange integrals, and *F* is the vibrational overlap factor. The values of the intermolecular transfer integrals at different pressures are given in Table IV. The bandwidths in $a^{-1}$, $b^{-1}$ and $c^{-1}$ directions at different pressures are given in Table V. These were calculated from the *ITS* in Table IV. Figures 2 and 3 show the bandwidths in these directions for an excess hole and an excess electron respectively.

TABLE II

Intermolecular exchange integrals in units of $10^{-4}$ ev.

| Pressure (kBars) | | | | | | | |
|---|---|---|---|---|---|---|---|
| Molecule # | Atm. | 1.0 | 2.0 | 3.0 | 4.0 | 5.0 | 6.0 |
| | | | | Hole | | | |
| 2 | −0.41 | −0.00 | 0.45 | 0.96 | 1.52 | 2.15 | 2.83 |
| 3 | 308.95 | 318.83 | 329.01 | 339.50 | 350.31 | 361.45 | 372.93 |
| 4 | −2.17 | −2.28 | −2.40 | −2.52 | −2.65 | −2.79 | −2.93 |
| 5 | −1.39 | −1.46 | −1.52 | −1.59 | −1.67 | −1.74 | −1.82 |
| 6 | −36.20 | −39.85 | −43.83 | −48.18 | −52.92 | −58.09 | −63.73 |
| 7 | −1.69 | −1.82 | −1.96 | −2.11 | −2.28 | −2.45 | −2.64 |
| 8 | −0.28 | −0.30 | −0.31 | −0.32 | −0.34 | −0.35 | −0.36 |
| 9 | −118.94 | −127.15 | −135.81 | −144.92 | −154.52 | −164.62 | −175.26 |
| 10 | 108.27 | 114.49 | 120.93 | 127.56 | 134.39 | 141.41 | 148.59 |
| 11 | 0.12 | 0.13 | 0.14 | 0.15 | 0.15 | 0.16 | 0.17 |
| 12 | 0.00 | 0.00 | 0.00 | 0.00 | 0.00 | 0.00 | 0.00 |
| 13 | 0.00 | 0.00 | 0.00 | 0.00 | 0.00 | 0.00 | 0.00 |
| 14 | −0.23 | −0.24 | −0.25 | −0.27 | −0.28 | −0.30 | −0.31 |
| | | | | Electron | | | |
| 2 | 8.74 | 10.28 | 11.91 | 13.64 | 15.46 | 17.38 | 19.41 |
| 3 | −64.12 | −66.72 | −69.41 | −72.20 | −75.10 | −78.11 | −81.22 |
| 4 | −0.36 | −0.38 | −0.40 | −0.42 | −0.45 | −0.47 | −0.50 |
| 5 | 0.29 | 0.33 | 0.38 | 0.44 | 0.50 | 0.57 | 0.65 |
| 6 | −7.43 | −8.42 | −9.52 | −10.76 | −12.15 | −13.71 | −15.46 |
| 7 | 0.32 | 0.35 | 0.39 | 0.42 | 0.46 | 0.50 | 0.55 |
| 8 | 0.16 | 0.17 | 0.18 | 0.18 | 0.19 | 0.20 | 0.21 |
| 9 | 132.17 | 134.64 | 137.06 | 139.42 | 141.72 | 143.94 | 146.08 |
| 10 | 7.26 | 8.66 | 10.17 | 11.80 | 13.54 | 15.41 | 17.41 |
| 11 | 0.17 | 0.17 | 0.18 | 0.19 | 0.20 | 0.21 | 0.22 |
| 12 | 0.00 | 0.00 | 0.00 | 0.00 | 0.00 | 0.00 | 0.00 |
| 13 | 0.00 | 0.00 | 0.00 | 0.00 | 0.00 | 0.00 | 0.00 |
| 14 | −0.07 | −0.07 | −0.07 | −0.08 | −0.08 | −0.09 | −0.10 |

TABLE III

Vibrational overlap integrals of naphthalene.

| $n$ | $\langle \chi^{00} \vert \chi^{+n} \rangle$ | $\vert \langle \chi^{00} \vert \chi^{+n} \rangle \vert^2$ |
|---|---|---|
| 0 | 0.7247 | 0.52519 |
| 1 | −0.5816 | 0.33822 |
| 2 | 0.3300 | 0.10894 |
| 3 | −0.1529 | 0.02338 |
| 4 | 0.0614 | 0.00376 |
| 5 | −0.0220 | 0.00048 |

TABLE IV

Intermolecular transfer integrals, (IRS − IE) · F, in units of $10^{-4}$ ev.

| Pressure (Kbars) | | | | | | | |
|---|---|---|---|---|---|---|---|
| Molecule # | Atm. | 1.0 | 2.0 | 3.0 | 4.0 | 5.0 | 6.0 |
| | | | | Hole | | | |
| 2 | 0.04 | −0.24 | −0.55 | −0.89 | −1.27 | −1.69 | −2.16 |
| 3 | −228.96 | −236.79 | −244.88 | −253.24 | −261.88 | −270.82 | −280.05 |
| 4 | 1.36 | 1.43 | 1.50 | 1.58 | 1.66 | 1.75 | 1.83 |
| 5 | 0.88 | 0.92 | 0.95 | 0.99 | 1.03 | 1.08 | 1.12 |
| 6 | 24.55 | 27.08 | 29.50 | 32.50 | 35.78 | 39.23 | 43.14 |
| 7 | 1.05 | 1.13 | 1.22 | 1.32 | 1.42 | 1.53 | 1.65 |
| 8 | 0.18 | 0.19 | 0.19 | 0.20 | 0.21 | 0.22 | 0.23 |
| 9 | 79.19 | 85.13 | 91.41 | 98.05 | 105.08 | 112.51 | 120.38 |
| 10 | −77.47 | −82.31 | −87.35 | −92.53 | −97.88 | −103.38 | −109.06 |
| 11 | −0.08 | −0.08 | −0.09 | −0.09 | −0.10 | −0.10 | −0.11 |
| 12 | 0.00 | 0.00 | 0.00 | 0.00 | 0.00 | 0.00 | 0.00 |
| 13 | 0.00 | 0.00 | 0.00 | 0.00 | 0.00 | 0.00 | 0.00 |
| 14 | 0.14 | 0.15 | 0.16 | 0.17 | 0.18 | 0.19 | 0.20 |
| | | | | Electron | | | |
| 2 | −7.20 | −8.36 | −9.59 | −10.89 | −12.28 | −13.74 | −15.28 |
| 3 | 48.56 | 50.65 | 52.82 | 55.08 | 57.43 | 59.88 | 62.44 |
| 4 | 0.22 | 0.24 | 0.25 | 0.26 | 0.28 | 0.29 | 0.31 |
| 5 | −0.18 | −0.20 | −0.22 | −0.26 | −0.31 | −0.35 | −0.40 |
| 6 | 4.75 | 5.40 | 6.06 | 6.87 | 7.79 | 8.89 | 10.05 |
| 7 | −0.21 | −0.23 | −0.25 | −0.27 | −0.29 | −0.31 | −0.34 |
| 8 | −0.10 | −0.11 | −0.11 | −0.12 | −0.12 | −0.12 | −0.13 |
| 9 | −99.30 | −101.58 | −103.82 | −106.05 | −108.26 | −110.44 | −112.58 |
| 10 | −5.09 | −6.21 | −7.41 | −8.67 | −10.00 | −11.43 | −12.93 |
| 11 | −0.10 | −0.11 | −0.11 | −0.12 | −0.12 | −0.13 | −0.14 |
| 12 | 0.00 | 0.00 | 0.00 | 0.00 | 0.00 | 0.00 | 0.00 |
| 13 | 0.00 | 0.00 | 0.00 | 0.00 | 0.00 | 0.00 | 0.00 |
| 14 | 0.04 | 0.05 | 0.05 | 0.05 | 0.05 | 0.06 | 0.06 |

## MOBILITY CALCULATIONS

Drift mobility components and Hall mobilities for the six different directions of the current and magnetic field were calculated using a procedure similar to that used by Elnahwy, *et al.*,[14] in their calculations on anthracene.

Tables VI and VII give the components of the drift mobility tensor at different pressures in the constant relaxation-time and constant-free-path approximations, respectively. Table VIII shows a comparison between the calculated mobility anisotropies, at atmospheric pressure, and the available experimental data for naphthalene.[10–12] It can be seen that, although both the constant $\tau$ and the constant $\lambda$ approximations tend to exaggerate the drift mobility anisotropy, the constant $\tau$ approximation does it to a somewhat

TABLE V

Bandwidths (in $10^{-4}$ ev) corresponding to the intermolecular transfer integrals, (IRS-IE) · F.

| Pressure (Kbars) | | | | | | | |
|---|---|---|---|---|---|---|---|
| Direction | Atm. | 1.0 | 2.0 | 3.0 | 4.0 | 5.0 | 6.0 |
| | | | | Hole | | | |
| $\tilde{a}^{-1}_{lower}$ | 118.73 | 134.13 | 149.57 | 168.46 | 189.40 | 212.14 | 237.61 |
| $\tilde{a}^{-1}_{upper}$ | 104.50 | 111.20 | 117.18 | 124.61 | 132.53 | 140.29 | 149.25 |
| $\tilde{b}^{-1}_{lower}$ | 887.87 | 913.65 | 939.78 | 965.88 | 992.14 | 1018.75 | 1045.30 |
| $\tilde{b}^{-1}_{upper}$ | 902.21 | 936.86 | 972.68 | 1010.52 | 1050.17 | 1092.25 | 1135.95 |
| $\tilde{c}^{-1}_{lower}$ | 731.03 | 779.32 | 828.79 | 881.75 | 936.97 | 993.55 | 1053.89 |
| $\tilde{c}^{-1}_{upper}$ | 509.70 | 538.77 | 570.03 | 600.33 | 630.90 | 661.78 | 693.12 |
| | | | | Electron | | | |
| $\tilde{a}^{-1}_{lower}$ | 401.99 | 413.22 | 424.74 | 435.73 | 446.56 | 457.15 | 467.62 |
| $\tilde{a}^{-1}_{upper}$ | 433.70 | 449.50 | 465.69 | 482.45 | 499.89 | 518.44 | 537.29 |
| $\tilde{b}^{-1}_{lower}$ | 224.30 | 229.56 | 234.75 | 239.71 | 244.47 | 249.50 | 253.96 |
| $\tilde{b}^{-1}_{upper}$ | 611.39 | 633.17 | 655.68 | 678.47 | 701.98 | 726.14 | 750.95 |
| $\tilde{c}^{-1}_{lower}$ | 50.33 | 61.31 | 73.19 | 85.24 | 97.64 | 110.55 | 124.08 |
| $\tilde{c}^{-1}_{upper}$ | 32.71 | 39.73 | 47.18 | 55.39 | 64.26 | 74.40 | 85.11 |

Following the notation given by Katz *et al.*[3], "lower" and "upper" correspond to the two energy bands $E_{\pm}(\vec{K})$.

TABLE VI

Components of the drift mobility tensor (constant $\tau$ approximation) corresponding to the transfer integrals (IRS-IE) · F*.

| Pressure (Kbar) | | | | | | | |
|---|---|---|---|---|---|---|---|
| Component | Atm. | 1.0 | 2.0 | 3.0 | 4.0 | 5.0 | 6.0 |
| | | | | Hole | | | |
| $\mu_{aa}$ | 36.81 | 41.09 | 45.74 | 50.91 | 56.51 | 62.56 | 69.25 |
| $\mu_{bb}$ | 606.31 | 631.28 | 656.44 | 682.07 | 708.13 | 735.03 | 761.95 |
| $\mu_{c'c'}$ | 108.49 | 118.51 | 129.16 | 140.54 | 152.62 | 165.15 | 178.85 |
| $\mu_{ac'}$ | −5.91 | −6.89 | −8.13 | −9.33 | −10.57 | −11.91 | −13.31 |
| | | | | Electron | | | |
| $\mu_{aa}$ | 123.10 | 126.46 | 129.81 | 133.04 | 136.21 | 139.39 | 142.44 |
| $\mu_{bb}$ | 76.22 | 79.20 | 82.29 | 85.43 | 88.71 | 92.08 | 95.61 |
| $\mu_{c'c'}$ | 3.19 | 4.44 | 5.99 | 7.88 | 10.11 | 12.79 | 15.90 |
| $\mu_{ac'}$ | −1.16 | −1.64 | −2.24 | −2.96 | −3.85 | −4.92 | −6.18 |

*All mobility components in units of $10^{10}$ $e\tau/kT$ $cm^2/V$-sec; $\tau$ in seconds, $e$ in coulombs and $kT$ in joules.

greater extent. This is in agreement with Leblanc's observation[18] that for conduction in narrow bands, the mean free path is constant rather than the relaxation time. The discrepancy between calculated anisotropy and experi-

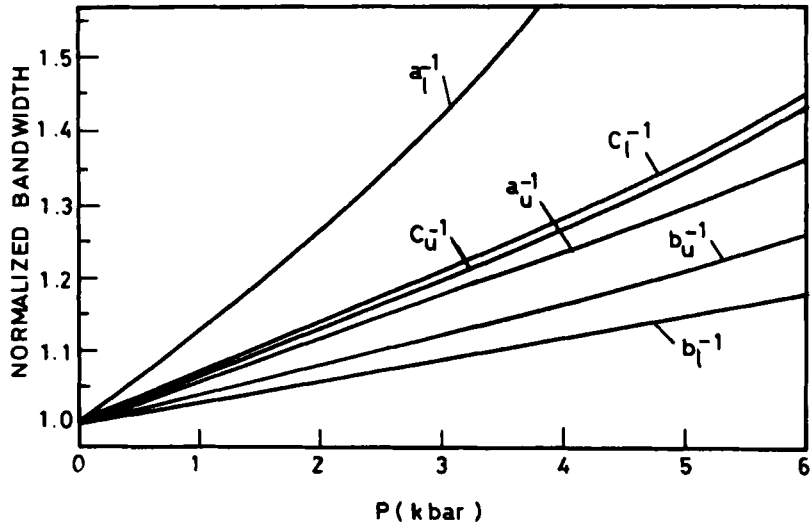


FIGURE 2 Normalized bandwidth for an excess hole.

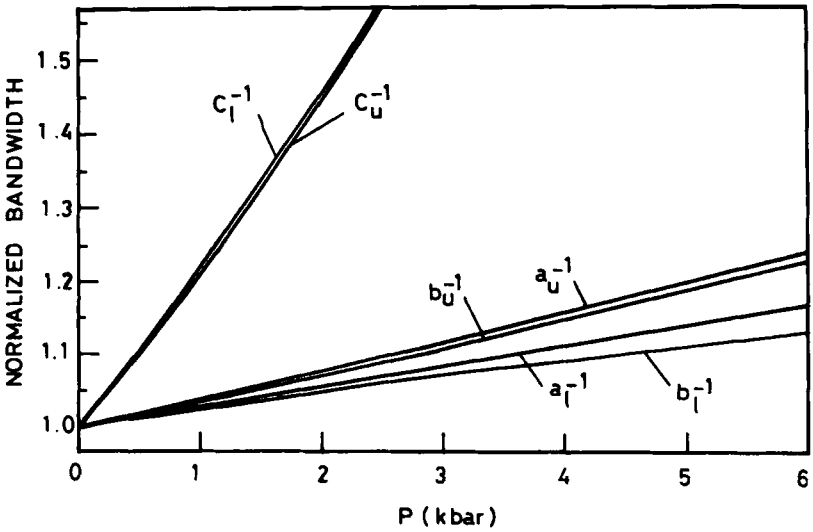


FIGURE 3 Normalized bandwidth for an excess electron.

ment is probably due to the assumption of an isotropic relaxation time. Kubarev and Mikhailov[19,20] suggested that the relaxation time in a particular direction is inversely proportional to the bandwidth in that direction. As shown in the last two columns of Table VIII, this in fact leads to a good

TABLE VII

Components of the drift mobility tensor (constant $\lambda$ approximation) corresponding to the transfer integrals (IRS-lE) · F[a].

| Pressure (Kbars) / Components | Atm. | 1.0 | 2.0 | 3.0 | 4.0 | 5.0 | 6.0 |
|---|---|---|---|---|---|---|---|
| | | | Hole | | | | |
| $\mu_{aa}$ | 1.263 | 1.376 | 1.495 | 1.626 | 1.765 | 1.911 | 2.070 |
| $\mu_{bb}$ | 18.839 | 19.087 | 19.326 | 19.558 | 19.786 | 20.018 | 20.230 |
| $\mu_{c'c'}$ | 3.581 | 3.820 | 4.066 | 4.323 | 4.589 | 4.855 | 5.142 |
| $\mu_{ac'}$ | −0.271 | −0.309 | −0.355 | −0.397 | −0.439 | −0.483 | −0.528 |
| | | | Electron | | | | |
| $\mu_{aa}$ | 7.654 | 7.717 | 7.769 | 7.810 | 7.841 | 7.863 | 7.873 |
| $\mu_{bb}$ | 4.877 | 4.942 | 5.007 | 5.071 | 5.135 | 5.200 | 5.266 |
| $\mu_{c'c'}$ | 0.334 | 0.448 | 0.582 | 0.736 | 0.908 | 1.102 | 1.317 |
| $\mu_{ac'}$ | −0.062 | −0.087 | −0.119 | −0.156 | −0.201 | −0.255 | −0.318 |

[a]All mobility components in units of $10^5$ e$\lambda/kT$ $cm^2$/V-sec; $\lambda$ in c$m$, $e$ in coulombs and $kT$ in joules.

TABLE VIII

Comparison of the drift mobility ratios of naphthalene in the anisotropic $\tau$ and the anisotropic $\lambda$ approximations.

| Ratio | Band width ratios[a] | Band width Exp.[b] | Mobility ratios const. $\tau$[c] | const. $\lambda$[c] | const. $\tau$ | const. $\lambda$ |
|---|---|---|---|---|---|---|
| | | | Hole | | | |
| *bb/aa* | 8.019 | 1.550 | 16.471 | 14.916 | 2.054 | 1.860 |
| *c'c'/aa* | 5.560 | 0.730 | 2.947 | 2.835 | 0.530 | 0.510 |
| | | | Electron | | | |
| *bb/aa* | 1.000 | 1.023 | 0.619 | 0.637 | 0.619 | 0.637 |
| *c'c'/aa* | 0.099 | 0.968 | 0.026 | 0.044 | 0.261 | 0.439 |

[a]The bandwidth ratios were taken from Table V

[b]Average of the drift mobility data published by Mey, *et al.*,[10] Silver *et al.*[11] and Spielberg *et al.*[12]

[c]The drift mobility ratios were taken from Tables VI and VII.

agreement with the anisotropies obtained from the experimental values of the drift mobility. Figures 4a,b and 5a,b, where *a* refers to holes and *b* to electrons, show the variation with pressure of the mobility tensors in the constant relaxation-time and constant mean free path respectively.

Tables IX and X give the calculated Hall mobility values for different directions of the current and magnetic field. Figures 6a,b and 7a,b show the variation of the Hall mobility with pressure.

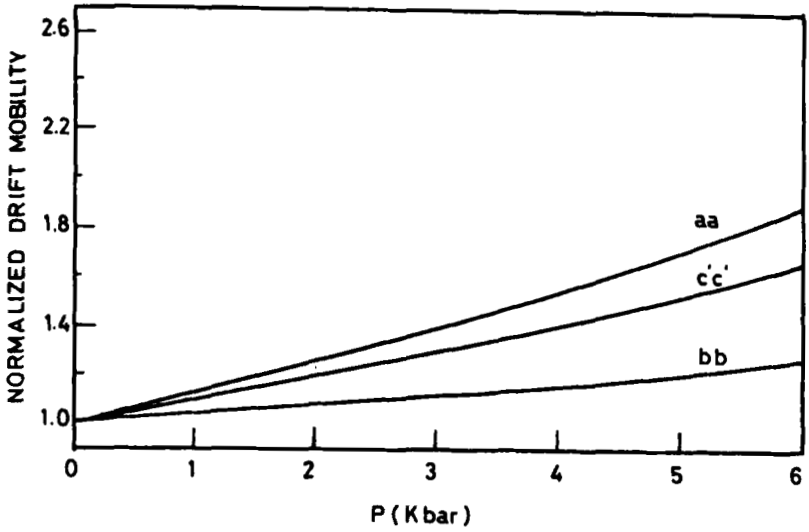


FIGURE 4a Normalized drift mobility for an excess hole in the constant relaxation time approximation.

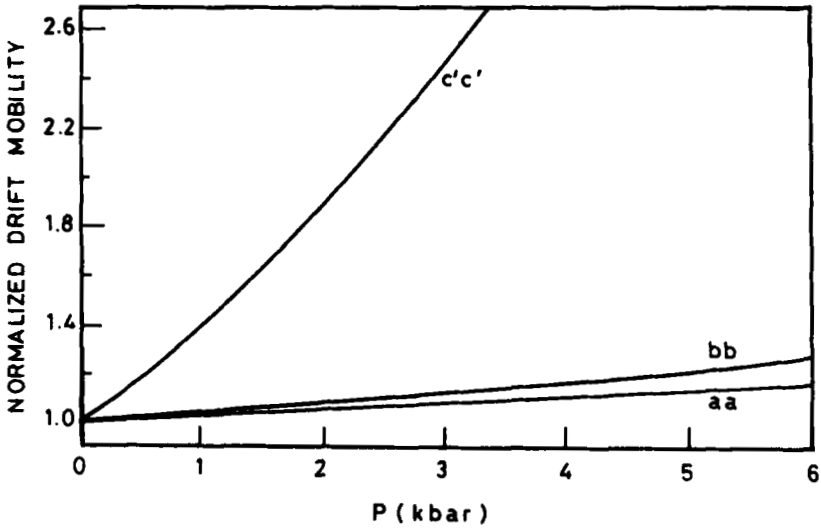


FIGURE 4b Normalized drift mobility for an excess electron in the constant relaxation time approximation.

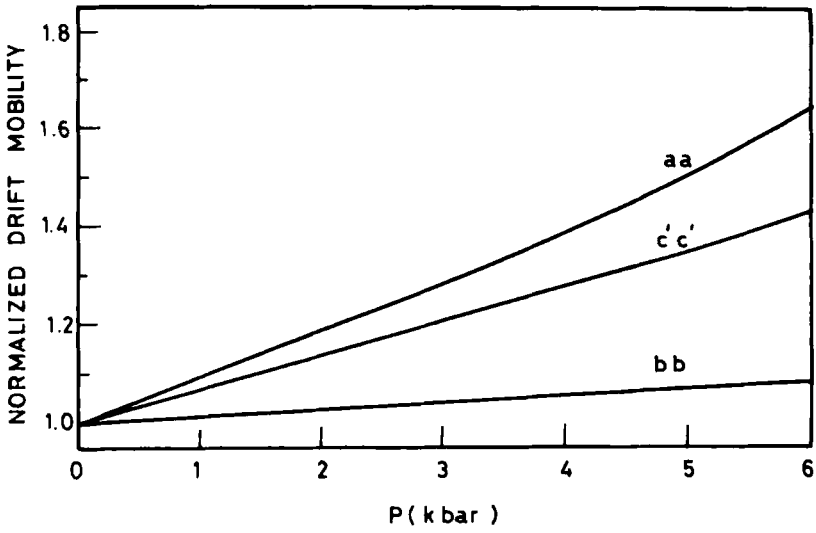


FIGURE 5a Normalized drift mobility for an excess hole in the constant mean free path approximation.

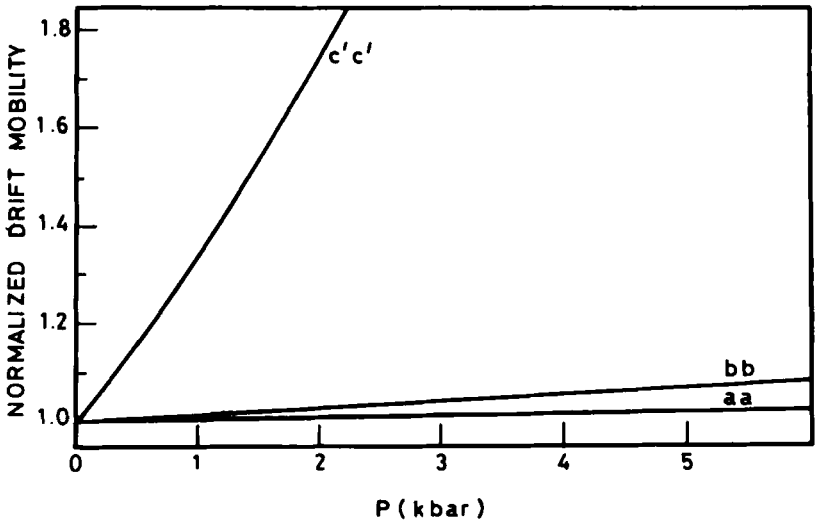


FIGURE 5b Normalized drift mobility for an excess electron in the constant mean free path approximation.

TABLE IX

Components of the Hall mobility tensor (constant $\tau$ approximation) corresponding to the transfer integrals (IRS-IE) · F[a].

| Pressure (Kbars) / Component[b] | Atm. | 1.0 | 2.0 | 3.0 | 4.0 | 5.0 | 6.0 |
|---|---|---|---|---|---|---|---|
| | | | Hole | | | | |
| $\mu_{13}$ | −0.128 | −0.134 | −0.139 | −0.143 | −0.146 | −0.148 | −0.148 |
| $\mu_{12}$ | 0.079 | 0.100 | 0.129 | 0.153 | 0.178 | 0.205 | 0.231 |
| $\mu_{23}$ | −2.115 | −2.055 | −1.994 | −1.917 | −1.830 | −1.736 | −1.630 |
| $\mu_{21}$ | −2.048 | −1.975 | −1.902 | −1.807 | −1.700 | −1.584 | −1.452 |
| $\mu_{32}$ | 0.232 | 0.288 | 0.364 | 0.423 | 0.480 | 0.541 | 0.597 |
| $\mu_{31}$ | −0.367 | −0.371 | −0.374 | −0.372 | −0.366 | −0.356 | −0.341 |
| | | | Electron | | | | |
| $\mu_{13}$ | 0.707 | 0.716 | 0.723 | 0.729 | 0.733 | 0.735 | 0.736 |
| $\mu_{12}$ | −0.786 | −0.849 | −0.905 | −0.937 | −0.962 | −0.975 | −0.986 |
| $\mu_{23}$ | 0.438 | 0.448 | 0.458 | 0.468 | 0.478 | 0.485 | 0.494 |
| $\mu_{21}$ | −0.309 | −0.308 | −0.307 | −0.305 | −0.303 | −0.300 | −0.297 |
| $\mu_{32}$ | −0.020 | −0.030 | −0.042 | −0.056 | −0.071 | −0.089 | −0.110 |
| $\mu_{31}$ | −0.013 | −0.017 | −0.022 | −0.028 | −0.035 | −0.042 | −0.049 |

[a]All mobility components in units of $10^{14}\tau$ $cm^2$/V-sec; $\tau$ in seconds.
[b]For $\mu_{ij}$, the first subscript $i$ indicates the direction of the applied electric field, while the second index $j$ corresponds to the direction of the magnetic field.

TABLE X

Components of the Hall mobility tensor (constant $\lambda$ approximation) corresponding to the transfer integrals (IRS-IE) · F[a].

| Pressure (Kbars) / Component[b] | Atm. | 1.0 | 2.0 | 3.0 | 4.0 | 5.0 | 6.0 |
|---|---|---|---|---|---|---|---|
| | | | Hole | | | | |
| $\mu_{13}$ | 0.309 | 0.361 | 0.409 | 0.465 | 0.527 | 0.594 | 0.684 |
| $\mu_{12}$ | 1.013 | 1.069 | 1.150 | 1.207 | 1.262 | 1.326 | 1.403 |
| $\mu_{23}$ | 4.617 | 5.004 | 5.282 | 5.593 | 5.907 | 6.226 | 6.679 |
| $\mu_{21}$ | 5.380 | 5.829 | 6.209 | 6.590 | 6.907 | 7.191 | 7.434 |
| $\mu_{32}$ | 2.872 | 2.969 | 3.127 | 3.209 | 3.281 | 3.369 | 3.484 |
| $\mu_{31}$ | 1.023 | 1.167 | 1.306 | 1.457 | 1.602 | 1.744 | 1.890 |
| | | | Electron | | | | |
| $\mu_{13}$ | −0.975 | −0.901 | −0.825 | −0.751 | −0.683 | −0.629 | −0.571 |
| $\mu_{12}$ | −14.552 | −13.525 | −12.484 | −11.665 | −10.983 | −10.375 | −9.870 |
| $\mu_{23}$ | −0.621 | −0.577 | −0.532 | −0.488 | −0.448 | −0.416 | −0.382 |
| $\mu_{21}$ | −6.356 | −6.027 | −5.754 | −5.530 | −5.343 | −5.169 | −5.008 |
| $\mu_{32}$ | −0.635 | −0.785 | −0.936 | −1.099 | −1.272 | −1.454 | −1.651 |
| $\mu_{31}$ | −0.435 | −0.546 | −0.669 | −0.802 | −0.944 | −1.096 | −1.252 |

[a]All mobility components in units of $10^7\lambda$ $cm^2$/V-sec; $\lambda$ in cm.
[b]For $\mu_{ij}$, the first subscript $i$ indicates the direction of the applied electric field, while the second index $j$ corresponds to the direction of the magnetic field.

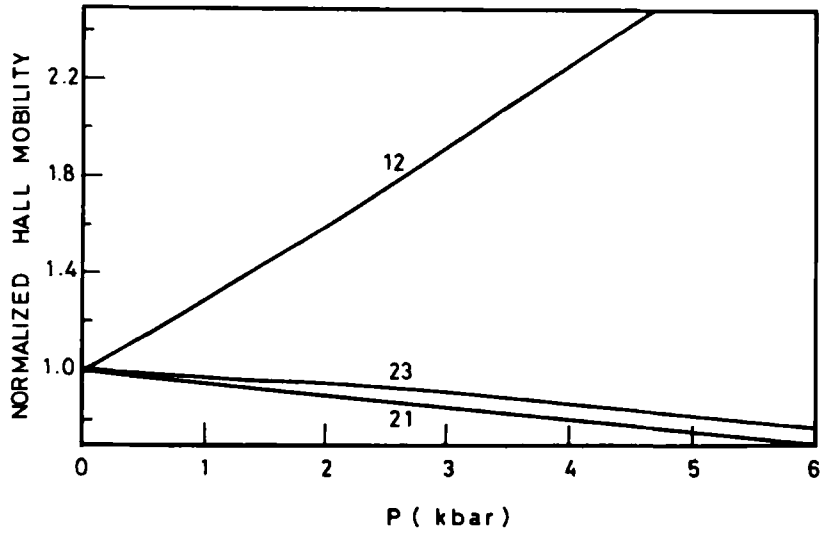


FIGURE 6a Normalized Hall mobility for an excess hole in the constant relaxation time approximation.

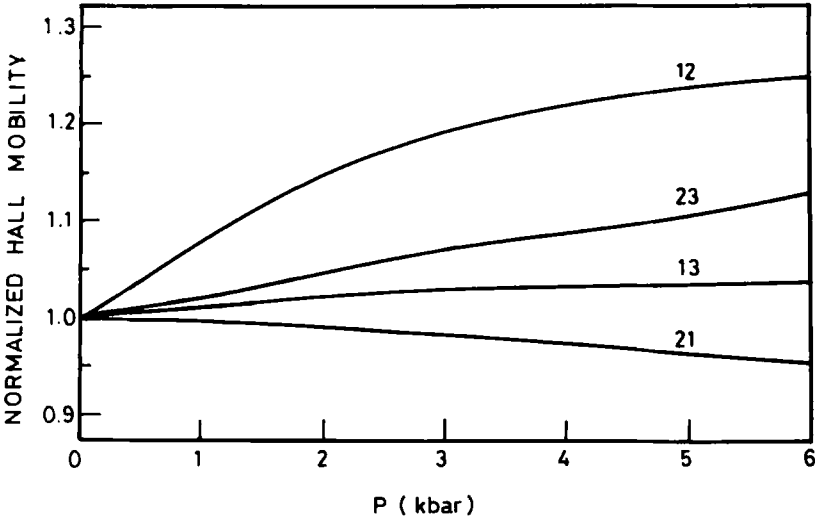


FIGURE 6b Normalized Hall mobility for an excess electron in the constant relaxation time approximation.

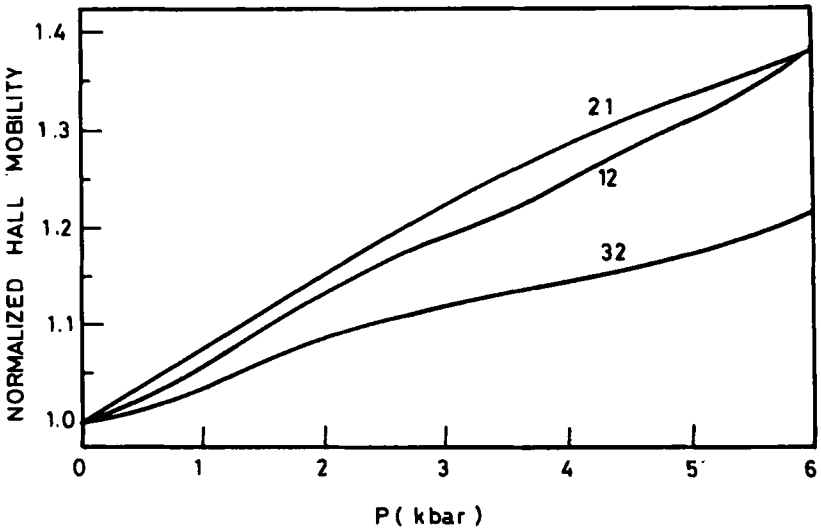


FIGURE 7a Normalized Hall mobility for an excess hole in the constant mean free path approximation.

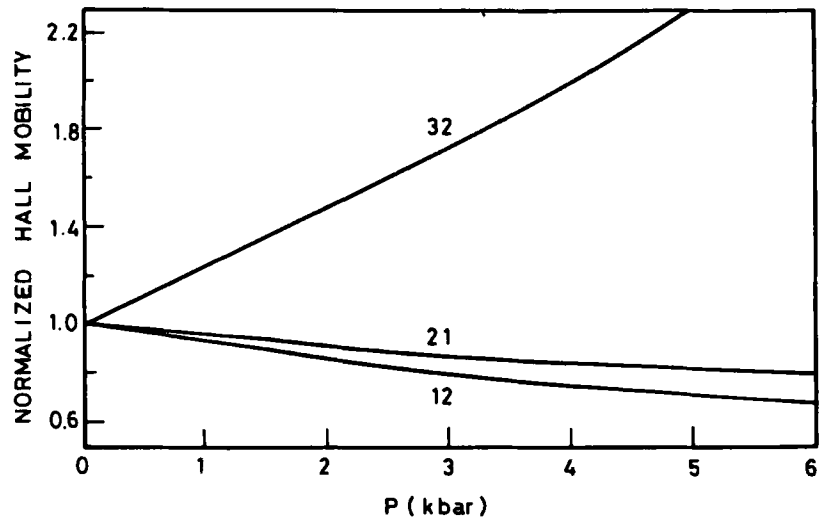


FIGURE 7b Normalized Hall mobility for an excess electron in the constant mean free path approximation.

## MEASUREMENT OF HALL MOBILITY OF AN EXCESS HOLE IN NAPHTHALENE AT HIGH PRESSURE

### Description of the experimental apparatus

(i) *Electrical system.* The electrical system used to measure the Hall effect was similar to the one developed by Korn *et al.*,[21] except for some slight modifications introduced to accomodate the restrictions imposed by high pressure measurements.

(ii) *Pressure measurement.* Pressure was measured by the variation in electrical resistance of a manganin wire. Manganin is a convenient alloy because of its linear rate of increase of resistance with pressure (0.4-13 kilobars) and also for its very low temperature coefficient of resistance.[22]

(iii) *The high pressure cell.* Measurement of Hall effect with optical injection at high pressure imposed certain special specifications on the design of the high pressure cell. Some of these specifications were: the cell material had to be nonmagnetic; the cell had to have two optical windows; and finally, the cell design had to provide five electrical connections from the high pressure side to the low pressure side. These are the electrical connections to the front electrode, back electrode, two Hall probes and the guard ring. The above design requirements were realized by the cell design shown in Figure 8. The cell was made of beryllium copper (#25 alloy). The material was chosen because of its non-permeability and strength, which was brought up to 176,000 psi by means of heat treatment at 600 °F for three hours after machining; its hardness was R. C. 37. The cell had two optically flat sapphire windows (c-axis within ±3°), 0.5 inch both in diameter and in thickness, purchased from Insaco; these allowed the uv radiation to reach the sample. The two windows, A and B, in the figure were kept in place by means of a hardened beryllium-copper Belleville spring which also provided the initial preloading on the windows. The spring had a 0.5 × 0.375 in. slot; the position of which was such that when plug C was tightened, the center of the slot fell exactly on the center line of plug D. This allowed the sample holder Figure 9 to fit easily inside the spring. The sample holder was supported by a stack, shown in Figure 10. The latter consisted of four lead rings and an end-piece to which the sample holder support was welded. The metallic rings were insulated from each other by means of four lucalox rings, purchased from Insaco.

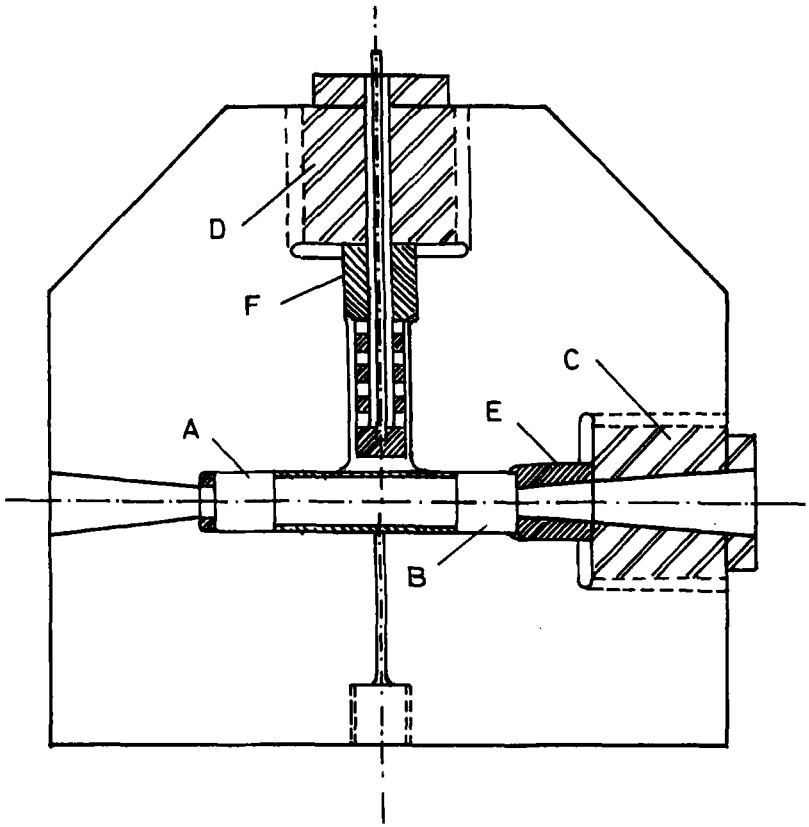


FIGURE 8 The high pressure cell.

Each of the four lead rings and the end piece had two teflon insulated wires soldered to it: one was soldered to its outer surface and went directly to one of the electrodes on the samples surface inside the cell; the second one was soldered to the inner surface of the ring (low pressure side) and connected to the Hall effect measuring equipment. The whole stack was held together by means of a teflon insulated rod.

(iv) *The crystal holder.* The crystal holder, shown in Figure 9, consisted essentially of a delrin base and a transparent electrode, both circular in shape, held together by means of eight brass screws and four brass sleeves. The transparent electrode was made of tin-oxide coated quartz. The screw holes in this electrode were drilled ultrasonically. The quartz

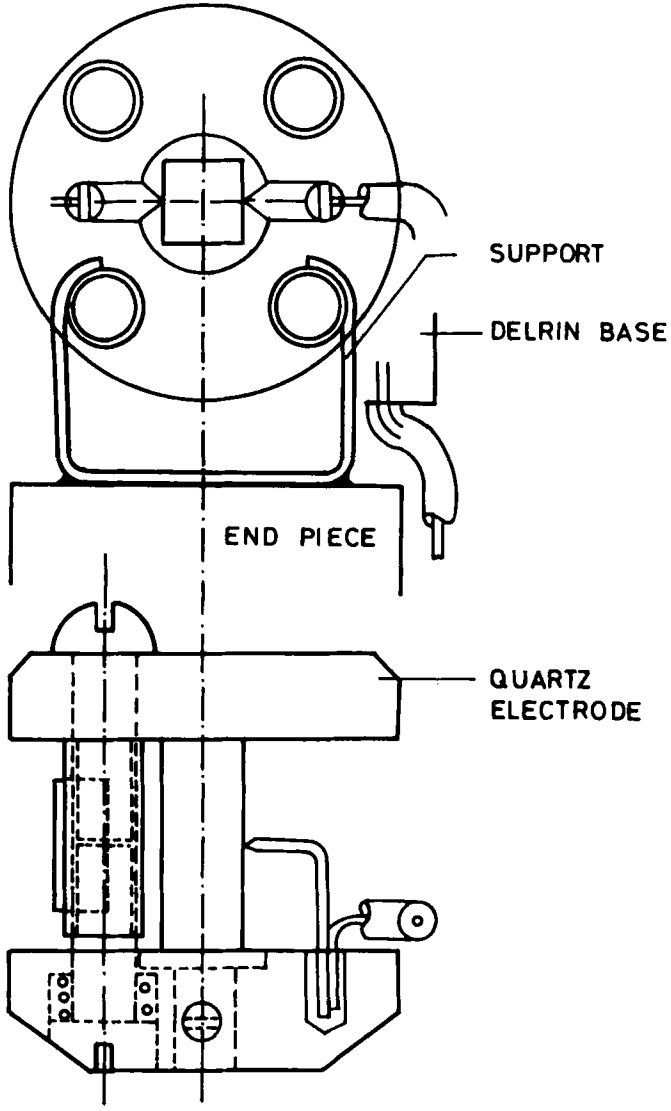


FIGURE 9 The sample holder.

electrode and the delrin base were spring loaded to insure good electrical contacts without breaking the sample. The dark electrode consisted of a copper platform snug-fitted into the delrin base.

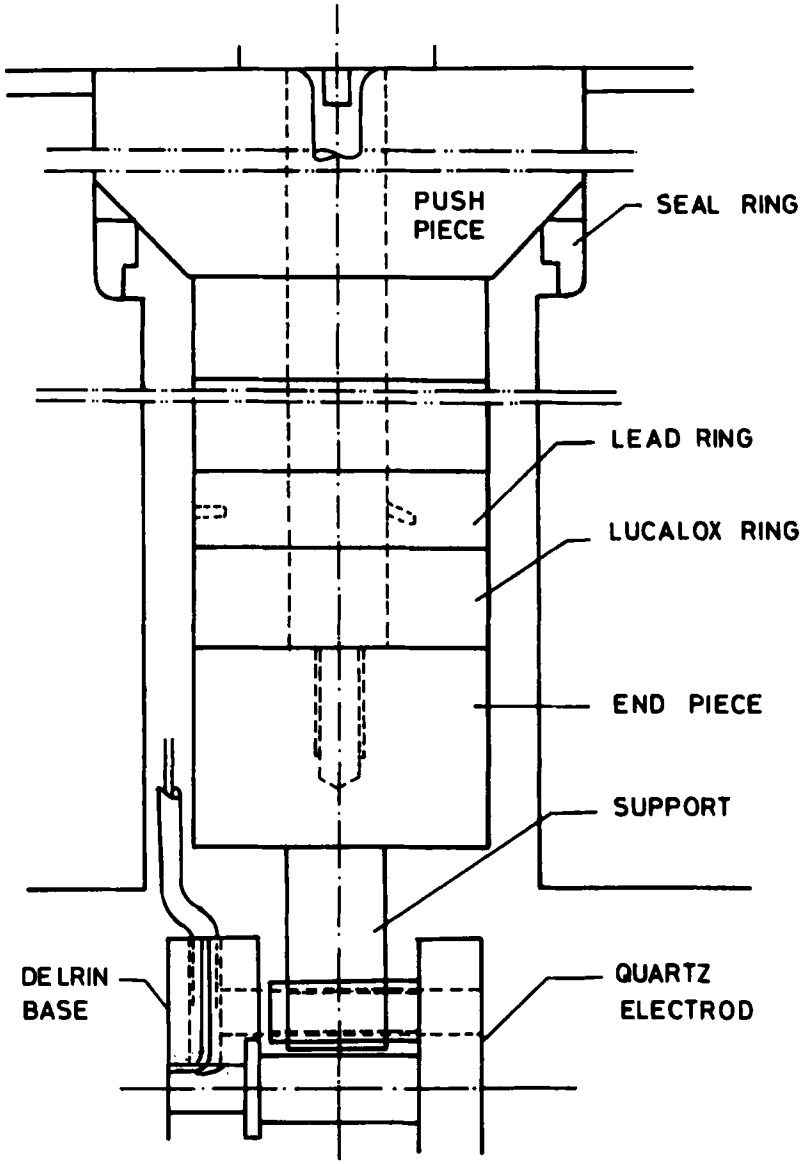


FIGURE 10 The stack supporting the sample holder.

(v) *The optical system.* A 1000 watt xenon lamp was used to illuminate the sample. A heat filter, in the form of quartz cell filled with water, was placed in the beam to reduce the amount of infra-red radiation getting to the sample.

**Techniques and results**

The shape of the samples used was similar to that used by Spielberg, *et al.*,[12] but half its linear dimensions.

After the high-pressure cell was introduced in the pole gap and the electronic system connected, argon was allowed to flow into the cell to keep the napththalene crystal at a pressure of about 10 atmospheres to slow the sublimation process. The leakage current was kept less than $10^{-13}$A by means of good insulation of the electrical contacts and a high degree of cleanliness of the delrin base and the surfaces of the lucalox rings. It was not possible to reduce the leakage current to the values reported by Spielberg, *et al.*,[12] namely, $10^{-15}$ to $10^{-14}$A because of the smaller dimensions of the sample holder in this work. Leakage currents prevented an accurate determination of the dark current. The guard ring was effective in eliminating surface currents. With the guard ring absent, the photo-current was typically an order of magnitude larger.

The Hall effect measurement began with adjusting the potential of the dark electrode, $V_D$, so that one of the Hall probes' potential was zero with respect to ground potential; the bucking potentiometers were then used to eliminate the imbalance of the Hall probe potentials. It was found that the electronic power supplies, in spite of their being regulated, caused large fluctuations in the photo-current and the Hall probes potential. Therefore, all three electrodes (the illuminated electrode, the guard ring and the dark electrode) were connected to mercury batteries.

The measurement was carried out by allowing for a sufficiently slow rate of drift to be achieved at the Hall probe. Such low rate was possible only at one Hall probe. At that point the chart recorder trace would indicate a zero magnetic field baseline. The magnetic field was then turned on, and as quickly as possible brought up to full strength. The time required to achieve full field was typically 10 to 20 seconds. The recorder would monitor the build-up in the Hall probe potential, until saturation occurred. The probe would then resume drifting with the slope of the initial drift for zero magnetic field. When the magnetic field was turned off, the Hall probe potential would revert back to the zero field baseline. A typical recorder trace is shown in Figure 11.

It was found that the Hall probe potential did not reverse its sign upon reversing the direction of the magnetic field. The Hall voltage corresponding to a certain value of the magnetic field was therefore taken to be the difference between the two signals obtained with the field in the normal and reverse directions, respectively. Among the six possible relative orientations of the electric and magnetic field, it was found that for the crystal geometry used, only two combinations of directions of the electric and magnetic fields gave reliable measurements of the Hall probe signal. These

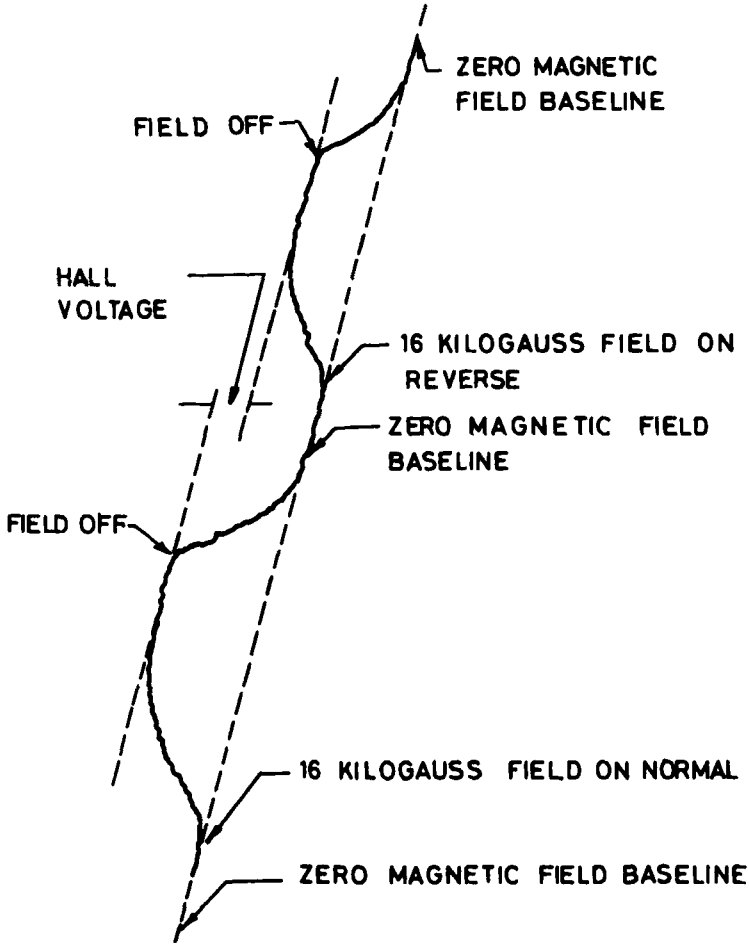


FIGURE 11 A typical chart recorder trace.

were for the electric field in the $a$ driection and the magnetic field in the $b$ direction ($\mu_{12}$), and reverse ($\mu_{21}$).

Measurements of Hall probe potential were carried out at various values of the magnetic field, and the results were plotted as a function of the field strength. Using a least-squares fitting routine, straight lines were found to provide a good fit to the data obtained from each direction of the magnetic field (normal or reverse). The Hall voltage, as function of the field strength, was then obtained as the difference between the two lines corresponding to the two opposite directions of the magnetic field.

The results at atmospheric pressure are given in Figures 12 through 15. The Hall probe signal as a function of the magnetic field is shown in

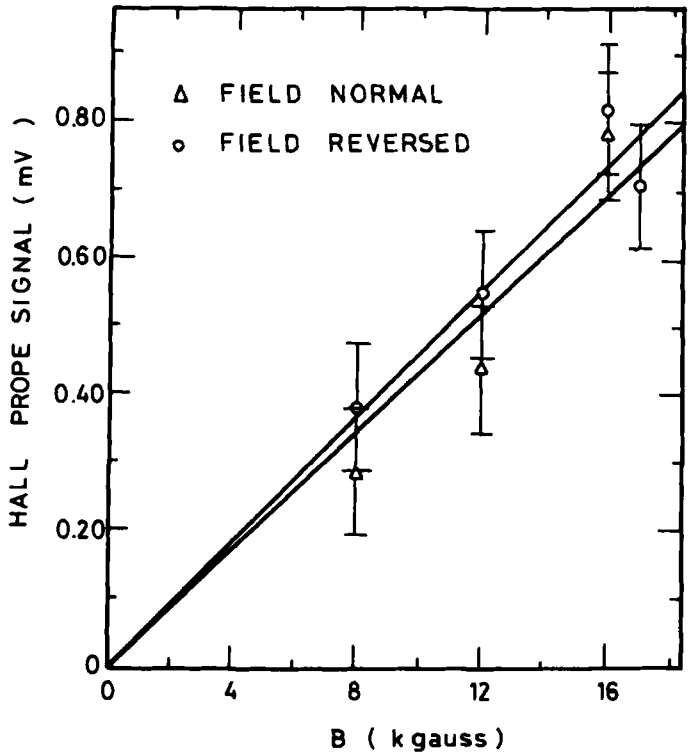


FIGURE 12 Hall probe signal for $\mu_{12}$ for an excess hole.

Figure 12, for the case of the electric field $E$ parallel to the crystal axis $b$ and the magnetic field $B$ parallel to $a$. The Hall voltage for this case is shown in Figure 13. Figures 14 and 15 give the Hall probe signal and the Hall voltage for the case of $E$ parallel to $a$ and $B$ parallel to $b$.

The measured Hall voltage $v_m$ was corrected for the finite sample dimensions and the space charge effects as follows:

$$v_H \text{ (corrected Hall voltage)} = \frac{2v_m}{GS}$$

where $G$ is the geometrical factor due to the finite sample dimensions[23] and $S$ is the space charge factor.[24]

The Hall mobility $\mu_H$ was then calculated from the relation,

$$\mu_H = \frac{v_H}{wE_xB_z}$$

Values of $\mu_{12}$ and $\mu_{21}$ at atmospheric pressure are given in Tables XI and XII respectively. Atmospheric and 2.2 kbar measurements had to be made

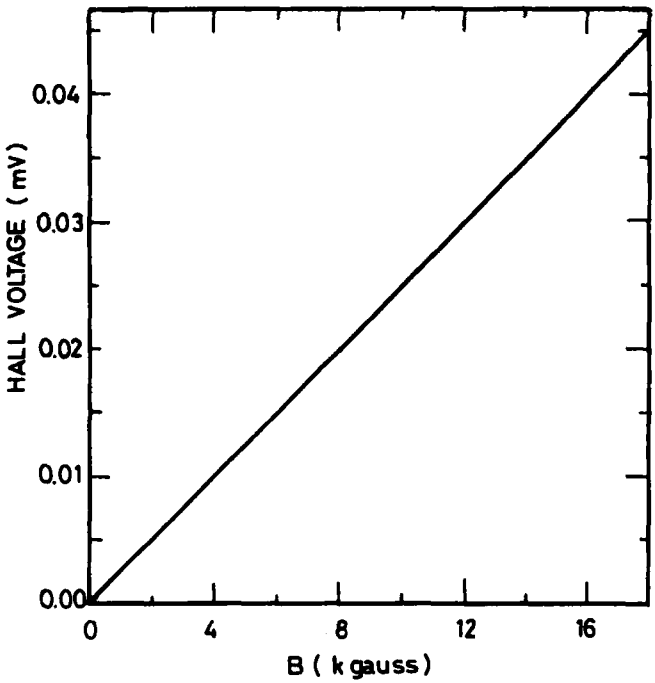


FIGURE 13 Hall voltage for $\mu_{12}$ for an excess hole.

in the same experiment on the same mounted crystal. Table XIII shows these values for $\mu_{12}$. It is seen that the value at atmospheric pressure is within the error limit of the value reported in Table XI.

All the above results were taken for an excess hole. No reliable measurements could be made for the Hall effect of electrons. The two Hall signals obtained for two opposite directions of the magnetic field were almost equal.

## Discussion of results

The absence of reversal in the sign of the Hall probe potential, upon reversing the direction of the magnetic field, had also been observed by Dresner[25,26] in the measurement of the photo-Hall effect of holes in anthracene. He attributed this effect to the presence of surface defects in his samples.

In the present work, the absence of reversal is interpreted in terms of the interaction between a triplet exciton (produced by intersystem crossover

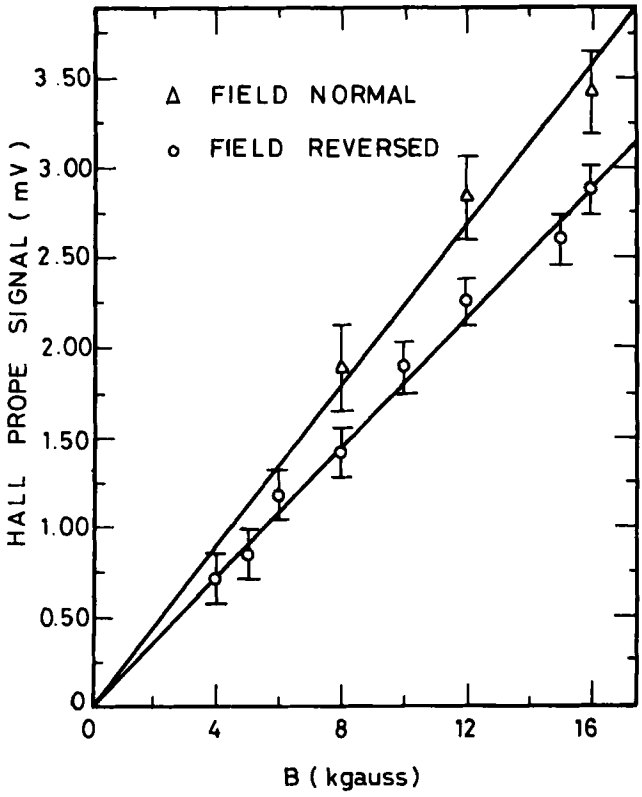


FIGURE 14 Hall probe signal for $\mu_{21}$ for an excess hole.

TABLE XI

Experimental data for the Hall mobility $\mu_{12}$ (current parallel to $a$, magnetic field parallel to $b$) at atmospheric pressure.

| $V_L$ (volt) | $V_D$ | Photocurrent ($10^{-12}$ amp) | $V_m/B_z$ (mv/kg) | $S$ | $G$ | $\mu_H$ ($cm^2$/V-sec) |
|---|---|---|---|---|---|---|
| 70 | 70 | 0.16 | 0.0025 | 0.0034 | 0.937 | 2.29 ± 1.20 |

$V_L$ is the positive bias applied to the illuminated electrode.
$V_D$ is the negative bias applied to the collecting electrode.
$V_m$ is the Hall voltage.
$B_z$ is the magnetic field intensity.
$S$ is the factor due to space charge effects.
$G$ is the geometrical factor due to the finite dimensions of the sample.

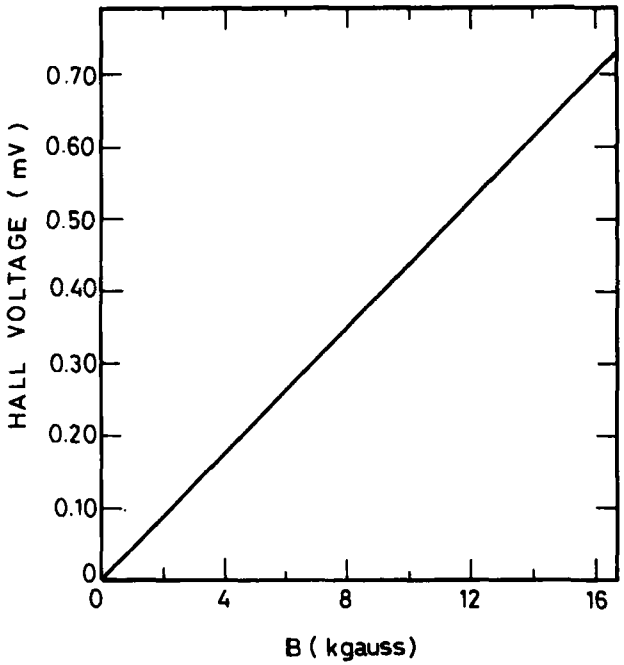


FIGURE 15 Hall voltage for $\mu_{21}$ for an excess hole.

TABLE XII

Experimental data for the Hall mobility $\mu_{21}$ (current parallel to $b$, magnetic field parallel to $a$) at atmospheric pressure.

| $V_L$ (volt) | $V_D$ | Photocurrent ($10^{-12}$ amp) | $V_m/B_z$ (mv/kg) | $S$ | $G$ | $\mu_H$ (cm$^2$/V-sec) |
|---|---|---|---|---|---|---|
| 70 | 70 | 0.25 | 0.044 | 0.00337 | 0.937 | 40.64 ± 8.18 |

$V_L$ is the positive bias applied to the illuminated electrode.
$V_D$ is the negative bias applied to the collecting electrode.
$V_m$ is the Hall voltage.
$B_z$ is the magnetic field intensity.
$S$ is the factor due to space charge effects.
$G$ is the geometrical factor due to the finite dimensions of the sample.

from a singlet state) and a trapped hole, in which process the triplet exciton is annihilated. In the presence of an external magnetic field, the triplet exciton-trapped hole interaction decreases, resulting in a change of the potential distribution in the crystal, including the region of the Hall probe. This change in the Hall probe potential is larger than the actual Hall

TABLE XIII

Experimental data for the Hall mobility $\mu_{12}$ (current parallel to $a$, magnetic field parallel to $b$) at atmospheric pressure and at 2.2 kilobars.

| $V_L$ (volt) | $V_D$ | Photocurrent ($10^{-12}$ amp) | $V_m/B_z$ (mv/kg) | $S$ | $G$ | $\mu_H$ (cm$^2$/V-sec) |
|---|---|---|---|---|---|---|
| | | | Atmospheric pressure | | | |
| 70 | 70 | 0.25 | 0.0031 | 0.0052 | 0.937 | 1.85 |
| | | | 2.2 kilobars | | | |
| 70 | 70 | 0.17 | 0.0027 | 0.0029 | 0.937 | 2.92 |

$V_L$ is the positive bias applied to the illuminated electrode.
$V_D$ is the negative bias applied to the collecting electrode.
$V_m$ is the Hall voltage.
$B_z$ is the magnetic field intensity.
$S$ is the factor due to space charge effects.
$G$ is the geometrical factor due to the finite dimensions of the sample.

voltage, and its sign is independent of the direction of the magnetic field. This interpretation is supported by the observation that when the injected carriers were electrons, the sign of the Hall probe potential was opposite to that obtained when holes were the injected carriers, thus indicating an interaction between triplet excitons and trapped electrons. The interaction between triplet excitons and trapped carriers was first reported by Geacintov, *et al.*,[27] and Frankevich, *et al.*,[28] to explain the effect of the magnetic field on the change in the photoconductivity of anthracene. Bouchriha, *et al.*,[29] and Pope, *et al.*,[30] gave similar interpretation in pyrene and tetracene, respectively. Bouchriha, *et al.*,[31] measured a decrease in the triplet exciton-trapped hole interaction, in anthracene, of up to 9% at 4.2 kilogauss. A result which is consistent with the interpretation of this work.

Referring back to Tables XI and XII, it can be seen that the Hall mobilities of holes, $\mu_{12}$ and $\mu_{21}$, both have a positive sign (non-anomalous effect). By comparing this result with the calculations (Tables IX and X), one notices that the band model in the constant $\lambda$ approximation agrees with it. The last conclusion is confirmed when the ratio

$$\frac{\mu_{12}\big|_{2.2kb}}{\mu_{12}\big|_{\text{atmospheric}}} = 1.58$$

is compared with the values predicted theoretically. One can see that the calculations carried out in the constant $\lambda$ approximation (Table X) give an increase of about 17%, while the calculations done in the constant $\tau$ approximation (Table IX) give an increase of about 70%. The latter calcu-

lations, however, give a negative sign for $\mu_{12}$ (holes) which contradicts the experimental data.

The discrepancy between the experimental value of 1.58, of the ratio of $\mu_{12}$ for holes at 2.2 Kilobars to its value at atmospheric pressure, and the value of 1.17 calculated in the constant $\lambda$ approximation can be explained by the uncertainty of about 30% occurring in the measurement of the Hall mobility $\mu_{12}$.

## Conclusion

The available Hall mobility data thus suggest that calculations carried out in the constant mean free path $\lambda$ approximation, taking into account the resonance and exchange integrals as well as the vibrational overlap, predict both the correct sign and, at least qualitatively, the variation with pressure of the Hall mobilities of holes in naphthalene.

This result, along with similar conclusions regarding the drift mobility tensor, therefore appear to favor a band conduction mechanism in naphthalene, where the mean free path, rather than the relaxation time, is constant.

## Acknowledgment

Appreciation is expressed to Prof. W. B. Daniels for designing the high pressure cell.

## References

1. O. H. Leblanc, Jr., *J. Chem. Phys.*, **35**, 1275 (1961); *36*, 1082 (1962).
2. G. D. Thaxton, R. C. Jarnagin and M. Silver, *J. Phys. Chem.*, **66** 2461 (1962).
3. J. L. Katz, S. A. Rice, S. I. Choi and J. Jortner, *J. Chem. Phys.*, **39**, 1683 (1963).
4. R. Silbey, J. Jortner, S. A. Rice and M. T. Vala, Jr., *J. Chem. Phys.*, **42**, 733 (1965); **43**, 2925 (1965).
5. R. M. Glaeser and R. S. Berry, *J. Chem. Phys.*, **44**, 3797 (1966).
6. K. Tanaka and K. Niira, *J. Phys. Soc. Japan*, **24**, 520 (1968).
7. O. H. Leblanc, Jr., *J. Chem. Phys.*, **39**, 2395 (1963).
8. L. Friedman, *Phys. Rev.*, **133**, A1668 (1964).
9. M. El Hamamsy, S. Elnahwy, A. C. Damask, H. Taub, W. B. Daniels, *J. Chem. Phys.*, **67**, 5501 (1977).
10. W. Mey and A. M. Hermann, *Phys. Rev. B*, **7**, 1652 (1973).
11. M. Silver, J. Rho, D. Olness and R. C. Jarnagin, *J. Chem. Phys.*, **38**, 3030 (1963).
12. D. H. Spielberg, A. I. Korn and A. C. Damask, *Phys. Rev. B*, **3**, 2012 (1971).
13. J. R. Hoyland, Ph. D. Thesis, Pennsylvania State University, 1961; J. R. Hoyland and L. Goodman, *J. Chem. Phys.*, **36**, 12 (1962).
14. S. A. Elnahwy, M. El Hamamsy, and A. C. Damask, *Phys. Rev. B*, **19**, 1108 (1979).
15. M. El Hamamsy, Ph.D. Thesis, The City University of New York (1976).
16. S. I. Choi, J. Jortner, S. A. Rice and R. Silbey, *J. Chem. Phys.*, **41**, 3294 (1964).

17. E. F. McCoy and I. G. Ross, *Australian J. Chem.*, **4**, 573 (1962).
18. O. H. Leblanc, Jr., Private Communication (1965) quoted in F. Gutmann and L. E. Lyons, Organic Semiconductors, p. 259, Wiley, New York (1967).
19. S. I. Kubarev and I. D. Mikhailov, *Theor. Exp. Chem.*, **3**, 265 (1967).
20. S. I. Kubarev and I. D. Mikhailov, *Theor. Exp. Chem.*, **4**, 134 (1968).
21. A. I. Korn, R. A. Arndt and A. C. Damask, *Phys. Rev.*, **186**, 938 (1969).
22. P. W. Bridgman, The Physics of High Pressure, p. 70, Dover Publications Inc., New York (1967).
23. I. Isenberg, B. R. Russel and R. F. Greene, *Rev. Sci. Inst.*, **19**, 685 (1949).
24. P. C. Banbury, H. K. Henisch and A. Many, *Proc. Phys. Soc.*, **66A**, 753 (1953).
25. J. Dresner, *Phys. Rev.*, **143**, 558 (1966).
26. J. Dresner, *J. Chem. Phys.*, **52**, 6343 (1970).
27. N. E. Geacintov, M. Pope and S. Fox, *J. Phys. Chem. Solids*, **31**, 1375 (1970).
28. E. L. Frankevich and I. A. Sokolik, *Solid State Commun.*, **8**, 251 (1970).
29. H. Bouchriha, M. Schott and J. L. Fave, *J. Phys. (Paris)*, **36**, 399 (1975).
30. M. Pope and Y. Solowiejczyk, *Molec. Cryst. Liq. Cryst.*, **30**, 175 (1975).
31. H. Bouchriha, G. Delacote, P. Delannoy and M. Schott, *J. Phys. (Paris)*, **35**, 577 (1974).